Amino Acid Substitutions in the Pore of the $Ca_V1.2$ Calcium Channel Reduce Barium Currents without Affecting Calcium Currents

Xianming Wang,* Tudor A. Ponoran,† Randall L. Rasmusson,‡ David S. Ragsdale,† and Blaise Z. Peterson*
*Department of Cellular and Molecular Physiology, The Pennsylvania State University College of Medicine, Hershey, Pennsylvania 17033; †Montreal Neurological Institute, McGill University, Montreal, Quebec H3A2B4, Canada; and ‡The Department of Physiology and Biophysics, University at Buffalo, The State University of New York, School of Medicine and Biomedical Sciences, Buffalo, New York 14214

ABSTRACT Ba^{2+} currents through $Ca_V1.2$ Ca^{2+} channels are typically twice as large as Ca^{2+} currents. Replacing Phe-1144 in the pore-loop of domain III with glycine and lysine, and Tyr-1152 with lysine, reduces whole-cell G_{Ba}/G_{Ca} from 2.2 (wild-type) to 0.95, 1.21, and 0.90, respectively. Whole-cell and single-channel measurements indicate that reductions in G_{Ba}/G_{Ca} result specifically from a decrease in Ba^{2+} conductance and not changes in V_h or P_O. Half-maximal block of I_{Li} is increased by 3.2-, 3.8-, and 1.6-fold in Ca^{2+}, and 3.8-, 4.2-, and 1.8-fold in Ba^{2+} for F1144G, Y1152K, and F1144K, respectively. High affinity interactions of individual divalent cations to the pore are not important for determining G_{Ba}/G_{Ca}, because the fold increases in IC_{50} values for Ba^{2+} and Ca^{2+} are similar. On the contrary, conductance-concentration curves indicate that G_{Ba}/G_{Ca} is reduced because the interactions of multiple Ba^{2+} ions in the mutant pores are altered. The complexity of these interactions is exemplified by the anomalous mole fraction effect, which is flattened for F1144G and FY/GK but accentuated for F1144K. In summary, the physicochemical properties of the amino acid residues at positions 1144 and 1152 are crucial to the pore's ability to distinguish between multiple Ba^{2+} ions and Ca^{2+} ions.

INTRODUCTION

Voltage-gated Ca^{2+} channels are important for the regulation of Ca^{2+} homeostasis, neurotransmitter release, muscle contraction, and gene expression. Voltage-activated Ca^{2+} channels are heteromultimeric complexes consisting of α_1, β, α_2/δ, and sometimes γ-subunits. The pore-forming α_1 subunit contains all of the structural determinants required for voltage-dependent gating, drug binding, and ion permeation (Fig. 1 *A*). The membrane topology of the α_1 subunit consists of four homologous domains (I, II, III, IV), each consisting of six transmembrane segments (S1–S6). The connecting segments between S5 and S6 of each domain contain negatively charged glutamate residues that line the pore of the channel and form a binding site for Ca^{2+} ions called the selectivity filter (1).

There are two fundamental properties that are essential for the function of voltage-gated Ca^{2+} channels: permeation and gating. Ion permeation through the pore of a Ca^{2+} channel is complex because the channel must be highly selective for Ca^{2+} ions, while maintaining an extremely rapid flux rate. The crystal structure of the bacterial K^+ channel, KcsA, has yielded valuable information about how K^+ channels selectively transport K^+ ions across the cell membrane (2–5), but the results of these studies shed little light on Ca^{2+} channel permeation for two main reasons: first, although the pores of Ca^{2+} and K^+ channels are likely to share gross structural features, their respective selectivity filters are undoubtedly distinct at the atomic level. Importantly, the K^+ channel pore is small, whereas the pore of the Ca^{2+} channel is very large (5,6) and selects Ca^{2+} ions over much more abundant ions such as Na^+ by binding Ca^{2+} ions with a high affinity. Second, the main chain carbonyl oxygen atoms project toward the lumen of the K^+ channel selectivity filter where they directly interact with K^+ ions (5), whereas the side chains of four negatively charged glutamate residues in the Ca^{2+} channel selectivity filter project toward the lumen of the pore (7–10) and form a single binding site (the EEEE locus) capable of binding a single divalent cation with a high affinity or two divalent cations with a low affinity (11–19). Since, the mechanisms by which ions selectively pass through the pores of the two channels are fundamentally different, one cannot rely on the structural details of the KcsA pore to develop an understanding of ion permeation through the Ca^{2+} channel pore. The Ca^{2+} channel pore appears to resemble that of other ion channels such as the Na^+ channels (19–22), so structural studies that reveal the molecular details of ion selectivity through Ca^{2+} channels are likely to have far-reaching applications to other classes of ion channels.

Ba^{2+} currents through L-type Ca^{2+} channels, as well as most other high voltage-activated Ca^{2+} channels, are approximately twice as large as Ca^{2+} currents (1,23,24). The differences between Ba^{2+} and Ca^{2+} conductance are thought to rely on the relative binding affinities single cations have for the selectivity filter (25–28). This phenomenon has been attributed to the observation that the binding affinity of a single Ba^{2+} ion to the selectivity filter is reported to be ~70-fold lower than that of Ca^{2+} (29). The repulsive forces exerted by the entry of a second ion are thought to promote the exit of a Ba^{2+} ion more readily than it would a Ca^{2+} ion—this increased exit rate manifests itself as an increase in ionic flux.

Submitted December 31, 2004, and accepted for publication June 22, 2005.
Address reprint requests to B. Z. Peterson, E-mail: bpeterson@psu.edu.

0006-3495/05/09/1731/13 $2.00
doi: 10.1529/biophysj.104.058875

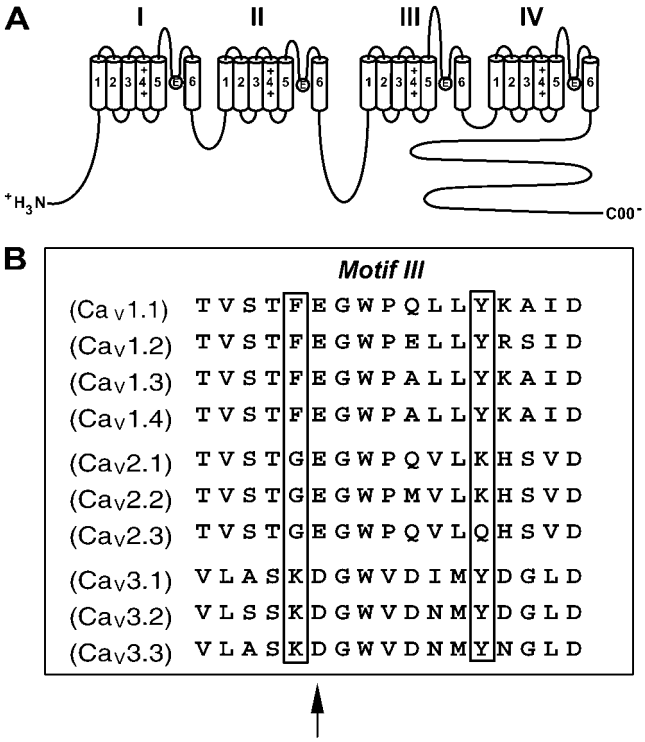

FIGURE 1 Phe-1144 and Tyr-1152 reside in the pore segment of domain III. (*A*) Transmembrane folding model of the α_1 subunit of high voltage-gated Ca^{2+} channels. The α_1 subunit consists of four homologous domains, each consisting of six transmembrane segments (S1–S6). Four glutamate residues, one residing in each of the four loops connecting S5 and S6 in each domain, form the selectivity filter, or EEEE locus. The selectivity filter is thought to bind a single divalent cation with a high affinity or multiple divalent cations with a low affinity. (*B*) Alignment of the domain III pore segment from each of the 10 Ca^{2+} channel family members. All high voltage-activated Ca^{2+} channels have a glutamate residue at position 1145, and all low voltage-activated Ca^{2+} channels have an aspartate residue at this position (*arrow*). All L-type Ca^{2+} channels ($Ca_V1.1$–4) have a phenylalanine, all high voltage-activated non-L-type Ca^{2+} channels ($Ca_V2.1$–3) have a glycine, and all low voltage-activated T-type Ca^{2+} channels ($Ca_V3.1$–3) have a lysine residue at position 1144 (*boxed*). All L-type Ca^{2+} channels ($Ca_V1.1$–4) and T-type Ca^{2+} channels ($Ca_V3.1$–3) have a tyrosine residue at position 1152, whereas two of three non-L-type Ca^{2+} channels ($Ca_V2.1$–2) have a lysine residue at this position.

Although current theoretical models are dependent on the binding-repulsion events in the pore (25–28), it should be noted that Ca_V3 channels exhibit a higher affinity for Ca^{2+} than Ba^{2+} (30) even though the two ions have similar conductances. Thus, how Ba^{2+} and Ca^{2+} ions traverse the pore appears to be more complex than these models predict.

Current models for selectivity and permeation through voltage-gated Ca^{2+} channels would predict that neutralizing the glutamate residues in the EEEE locus would have a direct effect on the channel's maximum conductance and that the magnitude of this effect would be proportional to the magnitude of the effect on cation binding to the selectivity filter. This has not proven to be the trend. Neutralization of only the fourth domain glutamate, Glu-IV, results in a reduction in the conductance for Ba^{2+} ions (18,31). This is surprising because, of the four glutamate residues, neutralization of Glu-IV has the smallest effect on the high affinity binding of divalent cations to the selectivity filter (16). Thus, although the EEEE locus appears to form a high affinity binding site for divalent cations, additional amino acids help determine the selectivity and permeability properties of the Ca^{2+} channel, as well.

Very little work has been done to establish how amino acids proximal to the EEEE locus influence permeation and selectivity (32,33). We have identified mutant Ca^{2+} channels with nonglutamate substitutions in the pore that alter specific permeation properties of the channel (33,34). Most notably, the ratio of Ba^{2+} to Ca^{2+} currents at -10 mV ($I_{Ba(-10)}/I_{Ca(-10)}$) is substantially reduced for all four mutants. The large reductions in $I_{Ba(-10)}/I_{Ca(-10)}$ result predominantly from a large reduction in G_{Ba} with little change in G_{Ca}. Measurements of half-maximal block of Li^+ currents indicate that reductions in G_{Ba}/G_{Ca} do not result from changes in high affinity occupancy of single divalent cations in the pore. Instead, our findings indicate that the magnitude of $G_{Ba(max)}/G_{Ca(max)}$ is dependent on complex interactions of multiple Ba^{2+} ions in the pore. The physicochemical properties of the amino acid residues at positions 1144 and 1152 are crucial to the pore's ability to distinguish between multiple Ba^{2+} ions and multiple Ca^{2+} ions.

EXPERIMENTAL PROCEDURES

Whole-cell patch-clamp recordings were acquired as described previously (35,36). Briefly, cDNAs encoding wild-type (37) and mutant $Ca_V1.2$ Ca^{2+} channels were cotransfected with β_{2a} (38), CaM_{1234} (35), and $\alpha_2\delta$ (39) into HEK293 cells by calcium phosphate precipitation. CaM_{1234} encodes an inactive form of calmodulin. Overexpression of CaM_{1234} has been shown to eliminate Ca^{2+}-dependent inactivation and facilitation of $Ca_V1.2$ channels (35,36,40,41). Therefore, CaM_{1234} was used in these experiments to eliminate complications that could arise from Ca^{2+}/CaM-dependent changes in channel gating. All cDNAs were expressed in the expression plasmid, pCDNA3 (Invitrogen, Carlsbad, CA).

Whole-cell currents were recorded at room temperature 2–3 days after transfection. Briefly, pipettes (2.5–3.5 MΩ) were pulled from borosilicate glass using a Sutter (Novato, CA) P-97 Flaming/Brown micropipette puller and fire polished on a MF200 microforge (World Precision Instruments, Sarasota, FL). Four types of external solutions were used for whole-cell recordings: 1), The external solutions for measuring Ca^{2+} and Ba^{2+} currents in Figs. 2–6 contained (in mM): *N*-methyl-D-glutamine (NMG)-aspartate, 130; HEPES, 10; 4-aminopyridine, 10; glucose, 10; and $CaCl_2$ or $BaCl^{2+}$, 10. The osmolarity was adjusted to 300 mmol/kg with sucrose and the pH was adjusted to 7.4. 2), The bath solutions for experiments where Ca^{2+}- or Ba^{2+}-dependent block of Li^+ currents was assessed (Figs. 8 and 9) contained (in mM): LiCl, 100; HEPES, 10; TEA-Cl, 14; EDTA, 5; HE-EDTA, 5; and $CaCl_2$ or $BaCl_2$, as needed based on published binding constants (WINMAXC, Chris Patton, Stanford University). The pH of these solutions was adjusted using TEA-OH, and the osmolarity was adjusted to 300 mmol/kg using TEA-Cl. 3), External solutions similar to those used in No. 1 were used in experiments that assess conductance-concentration relationships (Fig. 10), except that glucose and NMG were added or removed as necessary to maintain the desired osmolarity of 300 mmol/kg. 4), External solutions for assessing the anomalous mole fraction effect (AMFE) (Fig. 11) were identical to external solution No. 1, except that combinations of Ca^{2+} and Ba^{2+} were used to give the desired molar ratio of the two ions and the total divalent cation concentration was held at 2.0 mM. The internal solution for all experiments contained (in mM) NMG-$MeSO_3$, 140; EGTA, 10; $MgCl_2$, 1; Mg-ATP, 4; and HEPES, 10.

Data were acquired using a HEKA Epc9/2 amplifier and PULSE/PULSEFIT software. Currents were sampled at 10 kHz and low-pass filtered at 2 kHz. Series resistance was typically <6 MΩ and was compensated by ~70%. Leaks and capacitive transients were subtracted using a P/4 protocol. A custom-made rapid-exchange gravity-flow single-barrel single-cell perfusion system with an internal barrel diameter of ~0.2 mm was constructed that facilitated an exchange rate of <100 ms (data not shown). This apparatus was used in combination with a ramping protocol (−80 to +80 mV at a rate of 1 mV/ms) in Figs. 8 and 10. This approach greatly minimized complications resulting from current rundown, leak, and seal instability associated with Li^+ currents: entire dose-response curves were typically completed in <5 min with a high degree of reproducibility and little or no rundown. This approach assumes that changes in peak current reflect changes in permeation and not gating. Most of the solutions used in these studies are balanced such that junction potentials in 10 mM Ba^{2+} and Ca^{2+} are negligible (0.04 and 0.16 mV, respectively). Rather than correcting for junction potential offsets during the course of an experiment, junction potential offsets were ignored for experiments in Fig. 8 (where the junction potentials ranged from +7.4 to +9.2 mV as the divalent concentrations were increased from 5 nM to 10 μM in Ba^{2+}, and from +7.6 to +9.2 mV as the divalent concentrations were increased from 5 nM to 10 μM in Ca^{2+}) and Fig. 10 (where the junction potentials ranged from −2 to +12 mV as the divalent concentrations increased from 2 to 100 mM). Since the peak currents measured in Figs. 8 and 10 were obtained using a ramping protocol, the magnitudes of junction potential offsets for wild-type and mutant channels were the same. Thus, junction potentials did not affect the comparisons made in these studies.

Single-channel recordings were obtained using the patch clamp technique in the cell-attached configuration (42). For single Ca^{2+} currents, the pipette solution contained 110 mM $CaCl_2$, 10 mM HEPES, pH 7.5 with TEA-OH. To record single channel Ba^{2+} currents, $CaCl_2$ was replaced with 110 mM $BaCl_2$. The bath solution contained 140 mM potassium aspartate, 10 mM EGTA, 10 mM HEPES, pH 7.5 with KOH. Five micromolar Bay K 8644 was included in both the pipette and bath solutions in all recordings. Bay K 8644 is routinely used to prolong opening of single L-type calcium channels to facilitate measurement of single-channel current amplitudes. Bay K 8644 has previously been shown not to affect single-channel conductance (43–45), but see (46–51). No noticeable differences in current amplitudes were noted between patches with and patches without Bay K 8644, although in the absence of Bay K 8644 it was admittedly difficult to identify openings of long enough duration to resolve to make these judgments. Recordings were performed at room temperature, using an Axopatch 200B integrating patch clamp amplifier and pCLAMP software. Single-channel currents were elicited by 300 ms long depolarizations to potentials ranging from −30 mV to +30 mV, from holding voltages of −70 mV to −90 mV. Recordings were filtered at 1 kHz and sampled at 10 kHz.

Data are mean ± SEM. Error bars smaller than symbols do not appear in figures. Propagated errors were determined using conventional statistical approaches (52): $*p < 0.05$; $**p < 0.005$; $***p < 0.0005$.

RESULTS

Alteration of nonglutamate residues in the pore segment of domain III reduces the channel's preference for passing Ba^{2+} currents over Ca^{2+} currents

All of the mutagenic studies to date indicate that the glutamate residue in the pore of domain III is the most important determinant for ion permeation and selectivity (11–13,15–18). An alignment of the domain III pore segments from all 10 families of voltage-gated Ca^{2+} channels (Fig. 1 *B*) indicates that this segment is highly conserved. Note that all L-type Ca^{2+} channels ($Ca_V1.1$–4) possess a phenylalanine at position 1144, located immediately adjacent to Glu-1145 (*arrow*), whereas all non-L-type high voltage-activated Ca^{2+} channels ($Ca_V2.1$–3) possess a glycine and all low voltage-activated Ca^{2+} channels ($Ca_V3.1$–3) possess a lysine at this position. Tyr-1152 is located eight residues downstream of Phe-1144. All L- and T-type Ca^{2+} channels possess a tyrosine at this position, whereas non-L-type high voltage-activated Ca^{2+} channels have either a lysine or a glutamine at this position. That Phe-1144 and Tyr-1152 may be important for permeation and/or gating was first suggested by our findings that Phe-1144 (34) and Tyr-1152 (Blaise Z. Peterson, unpublished results) are important molecular determinants for Ca^{2+}-dependent dihydropyridine (DHP) binding to L-type Ca^{2+} channels, whereas Gln-1149, positioned between Phe-1144 and Tyr-1152, is not important for Ca^{2+}-dependent DHP binding (Blaise Z. Peterson, unpublished results). That DHP and Ca^{2+} binding is cooperative and DHPs modulate the gating (53) and perhaps conductance ((46–51), but see (43–45)) properties of L-type Ca^{2+} channels suggests that the gating and/or conductance properties of the channels is dependent on the identity of the residues that occupy positions 1144 and 1152.

To test this hypothesis, single mutants were made by substituting glycine and lysine into positions 1144 and 1152, respectively, to make $Ca_V1.2$ more $Ca_V2.1$-like and substituting lysine into position 1144 to make $Ca_V1.2$ more Ca_V3-like. To determine whether positions 1144 and 1152 act cooperatively to generate the $Ca_V2.1$-like phenotype, the double mutant FY/GK was constructed by simultaneously substituting glycine and lysine into positions 1144 and 1152, respectively. Since Phe-1144 and Tyr-1152 are both located in the Ca^{2+} channel pore, we first assessed the permeability properties of the mutant channels by comparing the relative amplitudes of Ba^{2+} and Ca^{2+} currents through each of the mutant channels with wild-type (Fig. 2). As is indicated in the upper panels of Fig. 2 and the summarized data in Fig. 3, Ba^{2+} currents at −10 mV through wild-type L-type Ca^{2+} channels were typically ~2.6 times larger than Ca^{2+} currents measured at the same potential from the same cell. In contrast, the ratios of $I_{Ba(-10)}/I_{Ca(-10)}$ for F1144G and FY/GK were decreased to only 0.95 and 0.69, respectively. The $I_{Ba(-10)}/I_{Ca(-10)}$ values for Y1152K and F1144K were reduced to a lesser extent to 1.69 and 1.28, respectively. Therefore, nonglutamate substitutions in the pore segment of domain III are important for determining the channel's preference for passing Ba^{2+} ions over Ca^{2+} ions.

Small changes in voltage-dependent activation contribute to the observed changes in $I_{Ba(-10)}/I_{Ca(-10)}$ for the mutant Ca^{2+} channels

The amplitude of whole-cell currents at −10 mV can be described using the following relation: $I = n \times P_{(-10)} \times i_{(-10)}$, where n is the number of functional Ca^{2+} channels in the plasma membrane, $P_{o(-10)}$ is the single-channel open prob-

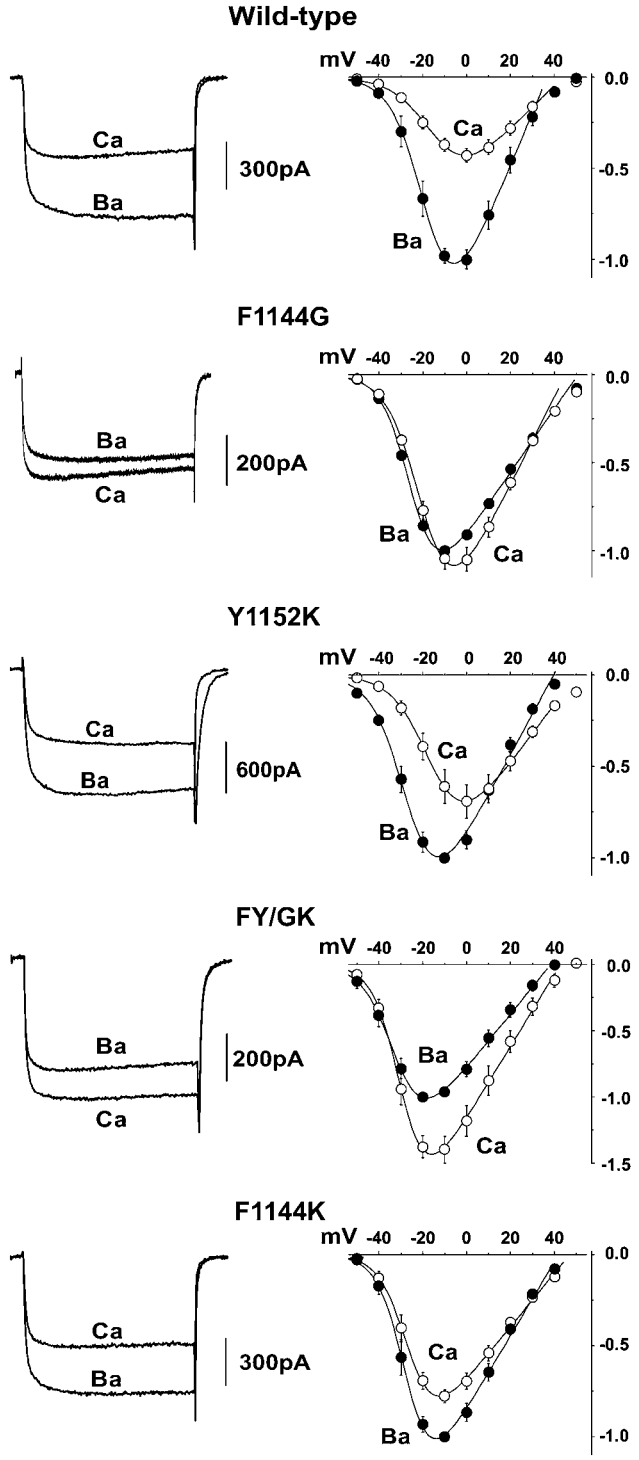

FIGURE 2 Alteration of nonglutamate residues in the pore segment of domain III reduces the channel's preference for passing Ba^{2+} currents over Ca^{2+} currents. (*Left*) Representative currents with 10 mM Ba^{2+} or 10 mM Ca^{2+} as the charge carrier. Currents were evoked by 150 ms step depolarizations to −10 mV from a holding potential of −90 mV. (*Right*) Current-voltage relations with Ba^{2+} (●) and Ca^{2+} (○) as the respective charge carriers are normalized to maximal Ba^{2+} currents recorded from the same cell and are plotted for comparison.

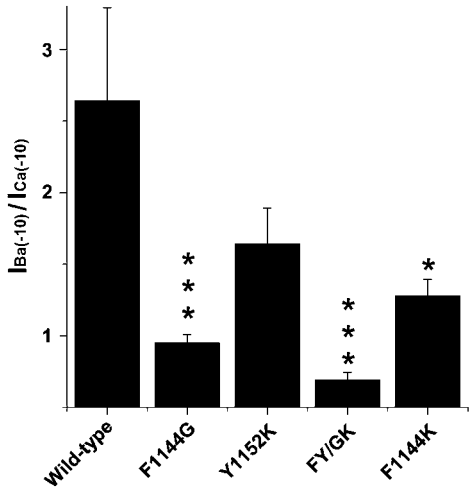

FIGURE 3 Substitutions in the pore have large effects on $I_{Ba(-10)}/I_{Ca(-10)}$. Quantitative analysis of data in Fig. 2. Ba^{2+} currents measured at −10 mV and were divided by Ca^{2+} currents measured at −10 mV to yield $I_{Ba(-10)}/I_{Ca(-10)}$. Note that replacing Phe-1144 with glycine or lysine results in large decreases in $I_{Ba(-10)}/I_{Ca(-10)}$, whereas modest effects are seen when Tyr-1152 is replaced by lysine. $I_{Ba(-10)}/I_{Ca(-10)}$ values: wild-type, 2.64 ± 0.65, $n = 6$; F1144G, 0.95 ± 0.06, $n = 8$; Y1152K, 1.64 ± 0.25, $n = 5$; FY/GK, 0.69 ± 0.06, $n = 5$; and F1144K, 1.28 ± 0.06, $n = 5$.

ability at −10 mV, and $i_{(-10)}$ is the single-channel current at −10 mV. Since $I_{Ba(-10)}/I_{Ca(-10)}$ is determined from the same cell, the number of channels does not change. Therefore, it is only necessary to determine whether relative changes in $P_{o(-10)}$ or $i_{(-10)}$ contribute to the observed changes in $I_{Ba(-10)}/I_{Ca(-10)}$ for the mutant channels.

The current-voltage relations of Fig. 2 (*right*) suggests that the estimated half activation voltage, V_h, may be altered for the mutant channels. The *I/V* relation for wild-type Ca^{2+} channels with Ca^{2+} as the charge carrier is typically shifted ~10 mV to the right of the *I/V* measured with Ba^{2+} as the charge carrier, an effect often attributed to differences in the shielding effects between the two ions (1). For Y1152K, V_h measured in Ba^{2+} is shifted slightly to the left compared to wild-type, whereas the V_h measured in Ca^{2+} is indistinguishable from that of wild-type. Such an ion-specific shift in gating could alter $I_{Ba(-10)}/I_{Ca(-10)}$ without changing the conductance of the channel for either ion. Likewise, *I/V* relationships measured with both Ba^{2+} and Ca^{2+} appear shifted to the left for FY/GK and F1144K.

Since changes in the voltage dependence of activation will directly affect $P_{o(-10)}$, we used a quantitative approach to assess how amino acid substitutions at positions 1144 and 1152 specifically affect this property. In Fig. 4, tail currents were evoked at −50 mV after 100 ms voltage steps to the indicated potentials. Tail currents measured with Ba^{2+} and Ca^{2+} as the respective charge carriers were normalized to the largest tail currents elicited in Ba^{2+}. These data, which reflect the voltage dependence of channel activation, show trends qualitatively similar to those observed with the *I/V* relations depicted in Fig. 2. For wild-type channels, V_h, the midpoint of

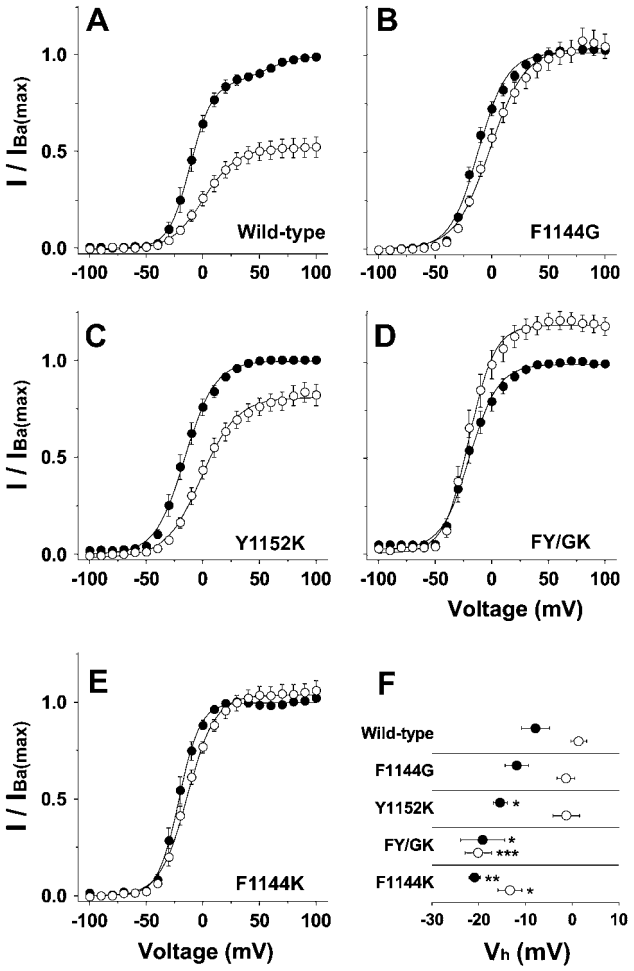

FIGURE 4 Substitutions in the pore segment of domain III produce small changes in the channel half-activation voltages. (*A–E*) Peak tail-currents were measured in Ba^{2+} (●) and Ca^{2+} (○) at −50 mV after 100 ms depolarizing potentials ranging from −100 to +100 mV. Smooth lines are single or double (wild-type, Ba^{2+}) Boltzmann fits through data normalized to $I_{Ba(max)}$. *F*. Mean V_h values derived from Boltzmann fits are plotted for wild-type and each mutant. V_h measured in Ba^{2+} (●): wild-type, −7.9 ± 3.1, $n = 6$; F1144G, −11.8 ± 2.1, $n = 8$; Y1152K, −15.4 ± 3.3, $n = 5$; FY/GK, −19.2 ± 3.5, $n = 5$; and F1144K, −20.9 ± 2.7, $n = 5$. V_h measured in Ca^{2+} (○): wild-type, +1.3 ± 2.5, $n = 6$; F1144G, −2.6 ± 1.7, $n = 8$; Y1152K, −1.8 ± 2.5, $n = 5$; FY/GK, −19.6 ± 3.0, $n = 5$; and F1144K, −14.2 ± 2.5, $n = 5$.

the tail-current/voltage curve measured with Ba^{2+} and Ca^{2+} as the charge carrier is −7.9 and +1.3 mV, respectively. For F1144G and Y1152K, V_h determined in Ca^{2+} is indistinguishable from wild-type. In Ba^{2+}, however, V_h for Y1152K is shifted 7 mV to the left. V_h determined with Ba^{2+} and Ca^{2+} as the charge carrier is shifted for FY/GK and F1144K: with Ca^{2+} as the charge carrier, V_h is shifted 21 and 16 mV in the hyperpolarizing direction, and V_h is shifted 11 and 13 mV in the hyperpolarizing direction when Ba^{2+} is the charge carrier for FY/GK and F1144K, respectively.

Although the negative shifts in V_h for Ba^{2+} and Ca^{2+} are about equal for F1144K, the changes in V_h observed for FY/GK and, to a lesser extent, Y1152K are asymmetrical. That is, V_h for FY/GK in Ca^{2+} is shifted 10 mV to the left more than V_h determined with Ba^{2+} as the charge carrier, and V_h for Y1152K in Ba^{2+} is shifted 4.4 mV to the left more than V_h determined when Ca^{2+} as the charge carrier. These ion-dependent changes in V_h suggest that ion binding in the pore can alter either the energetics of channel opening or local field potentials. That the phenotype of FY/GK does not simply reflect the sum of the effects on V_h for F1144G or Y1152K suggests that Phe-1144 and Tyr-1152 are codependent at determining the activation properties of the channel.

Although the effects on channel activation described above suggest that changes in $I_{Ba(-10)}/I_{Ca(-10)}$ (Figs. 2 and 3) result at least partially from changes in the voltage dependence of channel activation (V_h), Fig. 4 demonstrates that alterations in $I_{Ba(-10)}/I_{Ca(-10)}$ are dominated by factors other than V_h. In panels *A–E*, the $I/I_{Ba(max)}$ curves for Ca^{2+} were normalized to I_{max} for Ba^{2+} ($I_{Ba(max)}$). Normalizing the data in this way provides a means to compare maximal Ba^{2+} and Ca^{2+} currents from the same cell at voltages where P_O is maximal (e.g., +100 mV). It is evident that $I/I_{Ba(max)}$ for all four mutant channels differs substantially from that of wild-type. The bar plot in Fig. 5 provides a quantitative summary of the magnitudes to which $I_{Ba(max)}/I_{Ca(max)}$ is decreased for F1144G, Y1152K, FY/GK, and F1144K. It is noteworthy that significant effects on conductance of Y1152K are masked by the Ba^{2+}-specific shift in V_h depicted in Fig. 4 (compare Figs. 3 and 5).

Substitutions at positions 1144 and 1152 reduce channel Ba^{2+} conductance but have little effect on Ca^{2+} conductance

The $I/I_{Ba(max)}$ measurements in Figs. 4 and 5 indicate that changes in V_h are responsible for only a small fraction of the changes in $I_{Ba(-10)}/I_{Ca(-10)}$ for the mutant channels (Figs. 2 and 3). These experiments do not distinguish between changes in P_O and G, however, because at +100 mV where P_O is maximal, reductions in $I_{Ba(-10)}/I_{Ca(-10)}$ can occur if P_O in Ca^{2+} is increased, P_O in Ba^{2+} is decreased, Ba^{2+} conductance is decreased, or Ca^{2+} conductance is increased. To assess the conductance properties of F1144G, Y1152K, FY/GK, and F1144K in isolation, the maximal slope conductance was determined for wild-type and mutant channels using whole-cell instantaneous *I/V* relations (Fig. 6) and single-channel recordings (Fig. 7).

As expected for wild-type, I_{tail} is substantially larger at each potential in Ba^{2+} compared to that measured in Ca^{2+} (Fig. 6 *A*). This trend is depicted graphically in Fig. 6 *C*. Note that I_{tail} for Ba^{2+} (*solid circles*) is substantially larger than I_{tail} for Ca^{2+} at all potentials in the linear range. Note also, that the slope of the linear fit (the maximal slope conductance) is steeper for Ba^{2+} than it is for Ca^{2+}. The ratio of the maximal slope conductances in Ba^{2+} versus Ca^{2+} (G_{Ba}/G_{Ca}) for wild-type is 2.16 (Fig. 6 *H*), a value similar to

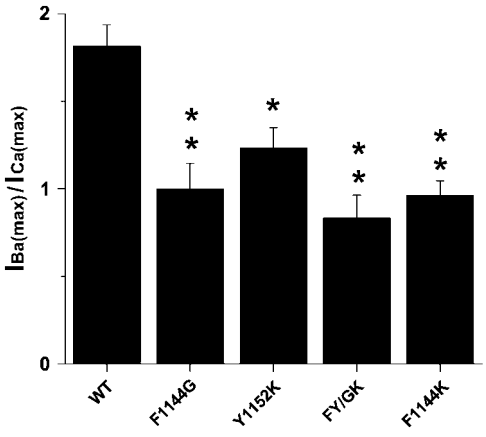

FIGURE 5 Changes in V_h contribute to the observed changes in $I_{Ba(-10)}/I_{Ca(-10)}$ for the mutant Ca^{2+} channels. Data in Fig. 4 were normalized to $I_{Ba(max)}$. The relationship between $I_{Ba}/I_{Ba(max)}$ and $I_{Ca}/I_{Ba(max)}$ can be seen in Figs. 4 and 5. In Fig. 5, $I_{Ba(max)}/I_{Ca(max)}$ is plotted as a bar graph so comparisons can be made with $I_{Ba(-10)}/I_{Ca(-10)}$ from Fig. 3. $I_{Ba(max)}/I_{Ca(max)}$ values: wild-type, 1.8 ± 0.12; F1144G, 1.0 ± 0.15; Y1152K, 1.23 ± 0.12; FY/GK, 0.83 ± 0.13; and F1144K, 0.96 ± 0.083.

the $I_{Ba(max)}/I_{Ca(max)}$ of 1.8 determined for wild-type in Fig. 5. F1144G shows a different trend. Note in panels *B* and *D* in Fig. 6 that I_{tail} in Ba^{2+} is similar to that determined in Ca^{2+} and that the linear fits through the two sets of data (i.e., the maximal slope conductances) are similar. These data are represented quantitatively in Fig. 6 *H* where G_{Ba}/G_{Ca} for F1144G is equal to 0.95, a value substantially lower than that for wild-type. Similar analyses were performed on Y1152K, FY/GK, and F1144K (Fig. 6, *E–G*), resulting in G_{Ba}/G_{Ca} values for Y1152K, FY/GK, and F1144K of 1.21, 0.95, and 0.90, respectively (Fig. 6 *H*).

The data in Figs. 4–6 demonstrate that changes in $I_{Ba(-10)}/I_{Ca(-10)}$ that result when Phe-1144 and Tyr-1152 are altered (Figs. 2 and 3) result primarily from changes in the channel's conductance properties and to a lesser extent V_h. By exclusion, P_O appears to play an insignificant role (note similarity between Figs. 5 and 6 *H*). It is not possible, however, to determine whether these substitutions reduce G_{Ba}/G_{Ca} by decreasing Ba^{2+} conductance or increasing Ca^{2+} conductance. To investigate how substitutions at positions 1144 and 1152 specifically affect the conductance of Ba^{2+} versus Ca^{2+}, single-channel recordings of wild-type and mutant channels were measured using 110 mM Ba^{2+} or 110 mM Ca^{2+} as the charge carriers. Fig. 7 *A* shows example single-channel traces, elicited at a test potential of −10 mV. Consistent with previous results (44), single-channel currents carried by Ba^{2+} were approximately twice as large as currents carried by Ca^{2+}. Mutation Y1152K had little effect on the relative amplitudes of Ca^{2+} versus Ba^{2+} currents; however, for mutants F1144G, F1144K, and FY/GK, Ba^{2+} currents were substantially reduced compared to wild-type. As a result, these mutant channels conducted Ca^{2+} and Ba^{2+} approximately equally well. To quantify this effect, we determined

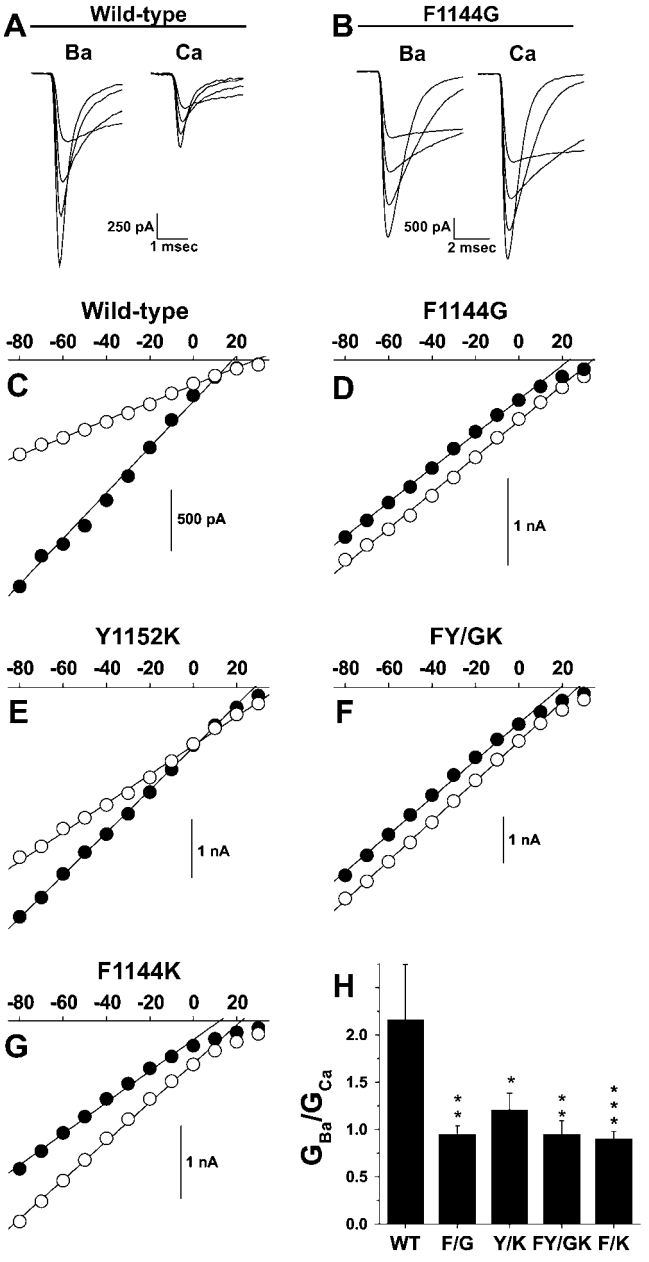

FIGURE 6 Whole-cell maximal slope conductances for F1144G, Y1152K, FY/GK, and F1144K are reduced. Whole-cell instantaneous *I/V* relations were generated by depolarizing wild-type and mutant cell membranes to +50 mV for 100 ms and then repolarizing them to test potentials ranging from −80 mV to +30 mV. (*A* and *B*) Tail currents evoked from repolarizing steps to −80, −60, −40, and −20 mV were generated in Ba^{2+} and Ca^{2+} from the same cell for wild-type (*A*) and F1144G (*B*). (*C–G*) Peak tail current amplitudes were measured in 10 mM Ba^{2+} (*solid symbols*) and 10 mM Ca^{2+} (*open symbols*) and plotted against the voltage of the repolarizing step. The linear portions of these data were fit using the equation $I_{tail} = G \times (V - E_{rev})$, where I_{tail} is the peak tail current, G is the maximal slope conductance, and E_{rev} is the reversal potential. Reversal potentials extrapolated by linear fits are more negative than their true reversal potentials, because the open channel *I–V* is nonlinear near the reversal potential for calcium channels. *H*. G_{Ba} is divided by G_{Ca} from the same cell to give G_{Ba}/G_{Ca}. Notice G_{Ba}/G_{Ca} values exhibit the same trends as $I_{Ba(max)}/I_{Ca(max)}$ values from Fig. 5: wild-type, 2.16 ± 0.58, n = 7; F1144G, 0.95 ± 0.087, n = 11; Y1152K, 1.21 ± 0.18, n = 8; FY/GK, 0.95 ± 0.14, n = 5; and F1144K, 0.90 ± 0.080, n = 9.

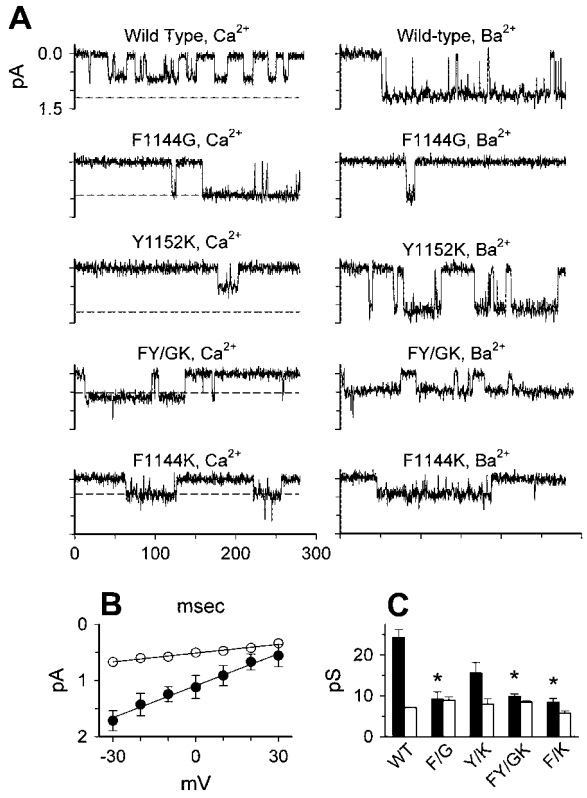

FIGURE 7 Mutants F1144G, F1144K, and FY/GK reduce single-channel Ba^{2+} currents but have little effect on single-channel Ca^{2+} currents. (*A*) Example traces, showing currents through single wild-type or mutant channels, with either 110 mM Ca^{2+} (*left*) or 110 mM Ba^{2+} (*right*) as the charge carrier. Currents were evoked by depolarizations to −10 mV. The dashed lines in the left-hand set of traces show the amplitudes of Ba^{2+} currents in the corresponding channel type, for comparison. (*B*) Mean current-voltage relationships for single wild-type channels, with Ca^{2+} (○) or Ba^{2+} (●). The straight lines are linear fits of the data points, with conductance values of 19.0 pS for Ba^{2+} and 7.1 pS for Ca^{2+}. (*C*) Summary of single-channel conductance values for Ba^{2+} (*solid bars*) versus Ca^{2+} (*open bars*). Conductance values were determined from the following numbers of patches: wild-type, Ca^{2+}, $n = 4$, Ba^{2+}, $n = 3$; F1144G, Ca^{2+}, 5, Ba^{2+}, 4; Y1152K, Ca^{2+}, 3, Ba^{2+}, 4; FY/GK, Ca^{2+}, 3, Ba^{2+}, 3; F1144K, Ca^{2+}, 4, Ba^{2+}, 3.

single-channel slope conductance values from linear fits of single-channel current amplitudes evoked at test potentials ranging from −30 mV to +30 mV (Fig. 7 *B*). These data are summarized in Fig. 7 *C*. As expected, for wild-type channels, Ba^{2+} conductance was 2.7 times larger than Ca^{2+} conductance (~19 vs. ~7.1 pS), whereas Ba^{2+} conductance values for F1144G, F1144K, and FY/GK were greatly reduced compared to wild-type and were approximately equal to Ca^{2+} conductance values. In addition to confirming our whole-cell data, these single-channel results demonstrate that mutations at position 1144 selectively reduce the maximal Ba^{2+} conductance of L-type Ca^{2+} channels while having little or no effect on maximal Ca^{2+} conductance. In the following sections, the mechanistic details that lead to these decreases in Ba^{2+} conductance are probed by measuring high and low affinity cation binding to the pore and the relationship between the two.

High affinity binding of single Ba^{2+} and Ca^{2+} ions to the selectivity filters of F1144G, Y1152K, FY/GK, and F1144K is reduced

Voltage-gated Ca^{2+} channels are highly selective for divalent cations (e.g., $P_{Ca}/P_K > 1000$; (1)) but become permeable to monovalent cations when divalent cations are removed from the bath. For example, large Li^+ currents are observed when cells expressing voltage-gated Ca^{2+} channels are perfused in a divalent-free bath solution (1). The robustness of these monovalent currents has been attributed to the fact that monovalent cations are not sufficiently charged to bind tightly to the negatively charged selectivity filter. Therefore, the dwell time for each permeant monovalent cation is short, resulting in a rapid flux rate. Low concentrations of divalent cations block monovalent currents such as Li^+ by interacting tightly with the selectivity filter and preventing the passage of Li^+ ions through the single-file pore.

The IC_{50} for half-maximal block of Li^+ currents by Ca^{2+} (Fig. 8, *A* and *C*) and Ba^{2+} (Fig. 8, *B* and *D*) was used to approximate the dissociation constants for the binding of single Ca^{2+} and Ba^{2+} ions to the selectivity filters of wild-type and mutant channels. As expected, the apparent IC_{50} for Ca^{2+} is 38-fold lower than that for Ba^{2+}. Substituting Phe-1144 with glycine increases the IC_{50} values for half-maximal block of Li^+ currents by Ca^{2+} (*open symbols*) and Ba^{2+} (*solid symbols*) by 3.2- and 3.8-fold, respectively. A smaller effect is observed when Phe-1144 is replaced by lysine: the IC_{50} for half-maximal block of Li^+ currents by Ca^{2+} and Ba^{2+} are increased by 1.6- and 1.8-fold, respectively. The largest effect for the single amino acid substitutions is seen when Tyr-1152 is changed to lysine and half-maximal block is increased 3.8- and 4.2-fold in Ca^{2+} and Ba^{2+}, respectively. Though not statistically significant, the IC_{50} values that result from combining F1144G and Y1152K (FY/GK) were consistently greater than either single mutant alone (4.1-fold in Ca^{2+} and 4.9-fold in Ba^{2+}).

The data in Fig. 8 are summarized in Fig. 9, where the IC_{50} values determined for each mutant are divided by the IC_{50} for wild-type to give the fold increases in Ba^{2+} (*solid bars*) and Ca^{2+} (*open bars*). Notice that the IC_{50} for half-maximal block of Li^+ currents by Ca^{2+} and Ba^{2+} is increased for F1144G, Y1152K, FY/GK, and F1144K, yet the fold increases in IC_{50} values for Ba^{2+} and Ca^{2+} each ion are similar for each mutant—i.e., the changes in the high affinity binding of individual divalent cations to the pores of the mutant channels are not ion specific. Note also that high affinity binding of individual divalent cations to Y1152K is more severely altered than it is to the other mutants with single amino acid substitutions, yet G_{Ba}/G_{Ca} for Y1152K is the least affected of the mutants (Figs. 6 and 7). Thus, even

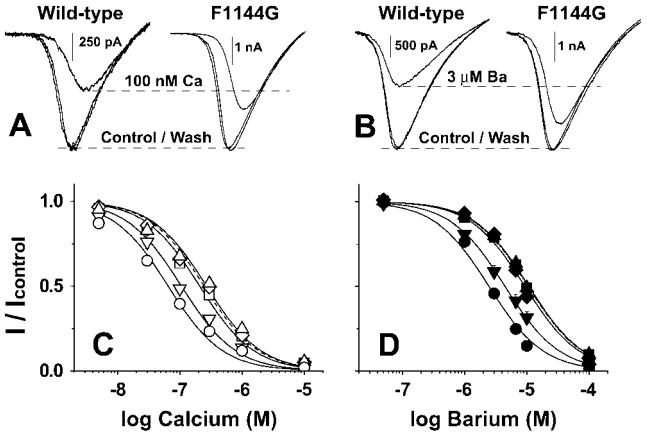

FIGURE 8 High affinity binding of single Ba^{2+} and Ca^{2+} ions to the selectivity filters of F1144G, Y1152K, FY/GK, and F1144K is reduced. (*A* and *B*) Block of Li^+ currents through wild-type (*left*) and F1144G (*right*) by 100 nM Ca^{2+} (*A*) and 3 μM Ba^{2+} (*B*). Currents were evoked using the ramping protocol described in Experimental Procedures. Peak currents measured at the indicated concentrations of free Ca^{2+} and Ba^{2+} were normalized to peak Li^+ currents recorded at nominal free divalent concentrations. That control currents superimpose with currents measured at the end of each experiment (*wash*) demonstrates that rundown of Li^+ currents was negligible. The small shifts in the *I/V* relations observed are likely due to ion-dependent effects on gating or voltage-dependent block. (*C* and *D*) Normalized Li^+ currents were measured in the presence of the indicated concentrations of free external Ca^{2+} (*C*) and Ba^{2+} (*D*). IC_{50} values determined in Ca^{2+} (nM): wild-type (●), 65 ± 7.6, $n = 7$; F1144G (■) 208 ± 24, $n = 4$; Y1152K (♦), 246 ± 28, $n = 4$; FY/GK (▲), 269 ± 31, $n = 5$; and F1144K (▼), 106 ± 12, $n = 4$. Block of Li^+ currents by Ba^{2+} (symbols and methods are the same as in *A*). IC_{50} in μM: wild-type, 2.47 ± 0.17, $n = 5$; F1144G, 9.37 ± 0.64, $n = 4$; Y1152K, 10.5 ± 0.73, $n = 5$; FY/GK, 12.1 ± 0.90, $n = 5$; and F1144K, 4.49 ± 0.29, $n = 4$.

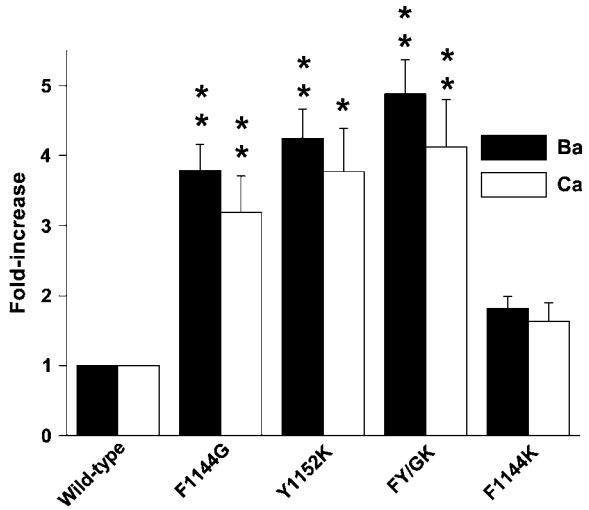

FIGURE 9 Differences in the binding affinities of individual Ba^{2+} and Ca^{2+} ions to the selectivity filter do not underlie the changes in G_{Ba}/G_{Ca} observed with the mutant channels. Fold increases in IC_{50} values for half-maximal block of Li^+ currents by Ba^{2+} (*solid*) and Ca^{2+} (*open*) are compared to wild-type. Note that mutant channels have reduced binding affinities for Ba^{2+} and Ca^{2+}, but the fold decreases in the high affinity binding for Ba^{2+} and Ca^{2+} are approximately equal.

though the residues at positions 1144 and 1152 are clearly important for determining the binding affinities of individual Ca^{2+} and Ba^{2+} ions to the selectivity filter, the changes we observe in the mutant channels' preferences for conducting Ba^{2+} over Ca^{2+} ions are not dependent on how single ions interact with the pore.

The relationship between saturating Ba^{2+} and Ca^{2+} currents is altered for F1144G and F1144K but not Y1152K

The data for F1144G, Y1152K, FY/GK, and F1144K in Figs. 8 and 9 indicate that the decreases in Ba^{2+} conductance does not result from changes in how individual Ba^{2+} ions interact with the pores of the mutant channels. Thus, it is likely that the substitutions have altered how multiple ions interact within the pores of the mutant channels. To test this, we compared the maximal slope conductances from currents generated in bath solutions containing Ba^{2+} or Ca^{2+} at concentrations ranging from 2 to 100 mM (Fig. 10). Notice in Fig. 10 *A* that the peak current is more than twice as large when 100 mM Ba^{2+} is the charge carrier than when 100 mM Ca^{2+} is the charge carrier. This is not the case for F1144G where peak currents in 100 mM Ba^{2+} and 100 mM Ca^{2+} are approximately equal (Fig. 10 *B*). In Fig. 10 *C–F*, the maximal slope conductances are determined for wild-type, F1144G, Y1152K, and F1144K at the indicated Ba^{2+} and Ca^{2+} concentrations and fit using the Michaelis-Menton equation. Saturating Ba^{2+} conductance through wild-type channels is ~2.3-fold larger than saturating Ca^{2+} conductance (Fig. 10, *C* and *G*). Saturating Ba^{2+} conductance relative to Ca^{2+} conductance is greatly reduced for F1144G and F1144K, yielding $G_{Ba(sat)}/G_{Ca(sat)}$ values of 0.89 and 0.51, respectively (Fig. 10, *D*, *F*, and *G*). Although $G_{Ba(sat)}/G_{Ca(sat)}$ for Y1152K was consistently smaller than wild-type, this difference was not statistically significant (Fig. 10, *E* and *G*). The K_S values for F1144G, F1144K, and Y1152K are not significantly different from wild-type (Fig. 10 *H*).

These results are in agreement with those in Figs. 6–9, indicating that the identity of the residues at positions 1144 and 1152 determine the magnitude of G_{Ba}/G_{Ca} by specifically altering how multiple Ba^{2+} ions interact in the pore. Although the single-channel data (Fig. 7) demonstrate that G_{Ba}/G_{Ca} is reduced for each of the mutant channels because Ba^{2+} conductance is reduced, the experiments in Fig. 10 demonstrate that G_{Ba} decreases because $G_{Ba(sat)}$ is decreased and not because K_S is increased.

The AMFE can be accentuated or attenuated by substituting Phe-1144 with glycine or lysine

The multi-ion nature of the Ca^{2+} channel pore has long been the subject of investigation. Hess and Tsien (26) and Almers and McCleskey (25) suggested that an electrostatic interaction between one ion bound to the channel and a

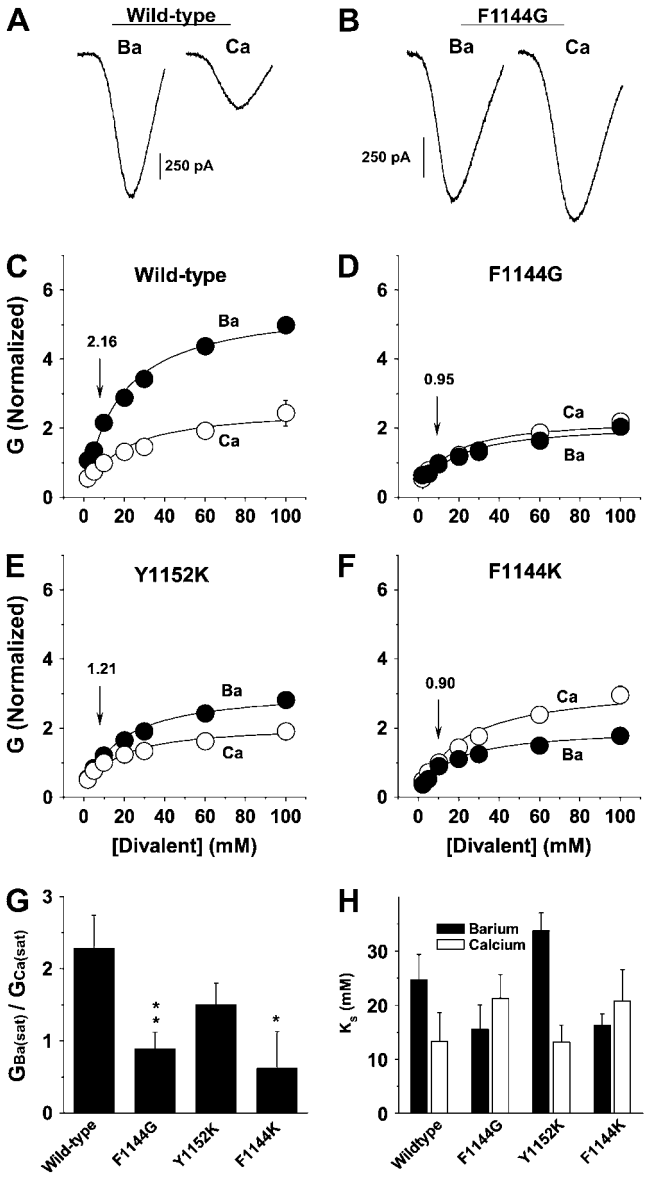

FIGURE 10 Relationship between saturating Ba^{2+} and Ca^{2+} conductance is altered for F1144G and F1144K. (*A* and *B*) Wild-type (*A*) and F1144G (*B*) currents with 100 mM Ba^{2+} (*left*) and 100 mM Ca^{2+} (*right*) as the respective charge carriers were evoked using the ramping protocol described in the Experimental Procedures. Notice that Ba^{2+} currents are more than twice the amplitude of Ca^{2+} currents for wild-type (*A*), whereas Ba^{2+} and Ca^{2+} currents through F1144G channels are about equal (*B*). (*C–F*) Maximal slope conductances were derived from fits through *I/V* relations measured at divalent concentrations ranging from 2 to 100 mM. Ba^{2+} (*solid symbols*) and Ca^{2+} (*open symbols*) were normalized by setting G_{Ca} measured in 10 mM Ca^{2+} to one and adjusting G_{Ba} measured in 10 mM Ba^{2+} to correspond with G_{Ba}/G_{Ca} determined in Fig. 6 *H* (numbers above *arrows* correspond to G_{Ba}/G_{Ca} in Fig. 6 *H*). This normalization procedure allows the direct comparison of the conductance-concentration curves at the whole-cell level with Ba^{2+} and Ca^{2+} as charge carriers. Maximal slope conductances were determined by Boltzmann fits using the equation, $I = G \times (V - E_{rev})/(1 + \exp((V - V_h)/K_S))$, where G is the maximal slope conductance, E_{rev} is the reversal potential, V_h is the half-activating potential, and K_S is the slope. It is not yet possible to express the relationship between divalent cation concentration and conductance in mathematical terms because such equations are model dependent and the molecular details of ion permeation through voltage-gated Ca^{2+} channels are still controversial (11,28,57,58). However, the Michaelis-Menton equation is frequently used to estimate the apparent dissociation constant for low affinity binding of divalent cations to the pore and to approximate the saturating conductance (23,24,44,50,57,65,66). Therefore, data are fit using the Michaelis-Menton equation, $G = G_{sat}/(1 + (K_S/c))$, where G_{sat} is the level of current at saturating concentrations of divalent cations, c is the concentration of divalent cation, and K_S is the divalent cation concentration that produces one-half G_{sat}. $G_{Ba(sat)}$: wild-type, 5.62 ± 0.34; F1144G, 2.13 ± 0.22; Y1152K, 3.12 ± 0.17; and F1144K, 1.99 ± 0.11. $G_{Ca(sat)}$: wild-type, 2.46 ± 0.28; F1144G, 2.39 ± 0.23; Y1152K, 2.09 ± 0.12; and F1144K, 3.21 ± 0.30. For comparison with data in Figs. 5–7, data are plotted as $G_{Ba(sat)}/G_{Ca(sat)}$ in panel *G*. (*H*) K_S values in mM are derived from Michaelis-Menton fits and plotted for Ba^{2+} (*solid bars*): wild-type 24.7 ± 4.6; F1144G 15.5 ± 4.5; F1144K 33.7 ± 3.3; and Y1152K 16.2 ± 2.1; and Ca^{2+} (*open bars*): wild-type, 13.3 ± 4.1; F1144G, 21.2 ± 6.8; F1144K, 13.2 ± 3.2; and Y1152K, 20.8 ± 5.7. Wild-type, $n = 4$; F1144G, $n = 4$; Y1152K, $n = 4$; and F1144K, $n = 4$.

second entering the pore occurs in Ca^{2+} channels. This results in a complex behavior of the conductance-activity relationship between the ions. An important demonstration of this interaction is a phenomenon called the AMFE. The AMFE occurs when a mixture of two permeant ions produces less current than either permeant ion alone. The AMFE is a complex phenomenon that depends on voltage and total concentration, as well as the intrinsic binding properties of the channel, and can be an important probe of ion-ion interactions in the open pore.

We studied the AMFE to examine how our mutations would affect ion-ion interactions in the open pore of Ca^{2+} channels. The experimental conditions were optimized to enhance our ability to detect changes in the AMFE. The AMFE was determined by measuring peak tail currents in the presence of various molar ratios of Ca^{2+} and Ba^{2+}. Consistent with other reports (54–56), we found that the AMFE was greatest when tail currents were evoked at relatively positive potentials (−30 mV) and when the total divalent cation concentrations were kept low (i.e., 2 mM). $I_{Ba(tail)}/I_{Ca(tail)}$ determined under these experimental conditions differs from $I_{Ba(max)}/I_{Ca(max)}$ determined using protocols described in Fig. 4. Furthermore, under conditions that promote the AMFE (2 mM divalent concentration and tail currents measured at −30 mV), $I_{Ba(tail)}/I_{Ca(tail)}$ values for the mutants do not follow the same trend as observed for G_{Ba}/G_{Ca} measured at −30 mV in Fig. 6. Together, these observations suggest that the extracellular divalent ion concentration is a critical parameter in determining the selectivity properties of the pore. For instance, notice in Fig. 11 that $I_{Ba(tail)}/I_{Ca(tail)}$ for F1144K is similar to that of wild-type and that $I_{Ba(tail)}/I_{Ca(tail)}$ for Y1152K is similar to that of FY/GK.

The AMFE for wild-type and mutant Ca^{2+} channels was measured using 2 mM mixtures of Ca^{2+} and Ba^{2+} such that the $Ba^{2+}/(Ba^{2+} + Ca^{2+})$ was 0.0, 0.3, 0.5, 0.7, 0.9, and 1.0 (Fig. 11). Note in Fig. 11 *B* that the normalized current for wild-type (*open circles*) decreases to 0.64 when $Ba^{2+}/(Ba^{2+}$

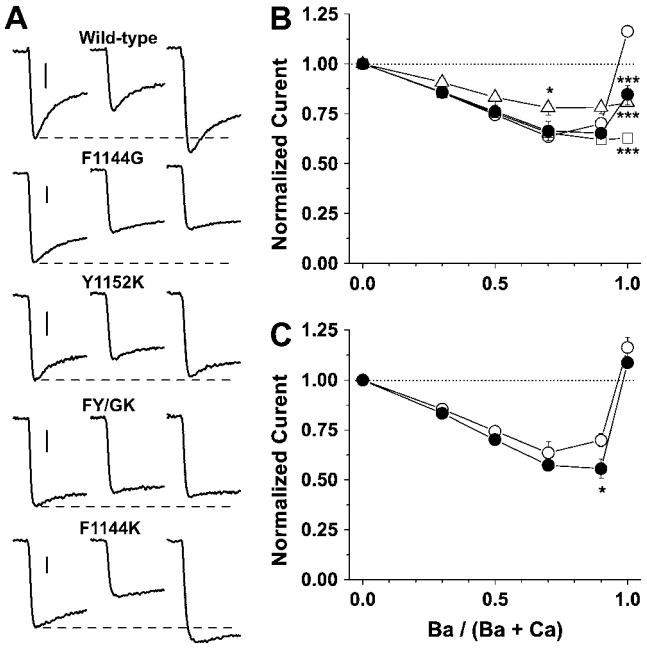

FIGURE 11 AMFE can be attenuated or accentuated by substitutions at Phe-1144. Cells were stepped from a holding potential of −90 to +50 mV for 100 ms, and peak tail currents evoked by stepping to −30 mV were measured at molar ratios of external Ba^{2+} to total divalent cation concentrations ($Ba^{2+}/(Ba^{2+} + Ca^{2+})$) of 0.0, 0.3, 0.5, 0.7, 0.9, and 1.0. The combined divalent concentration ($Ba^{2+} + Ca^{2+}$) at each data point was kept at 2 mM. (*A*) Sample peak tail currents for wild-type and mutant channels at $Ba^{2+}/(Ba^{2+} + Ca^{2+})$ ratios of 0 (*left*), 0.7 (*center*), and 1.0 (*right*). Dashed line corresponds to peak tail currents measured in an external solution containing 2.0 mM Ca^{2+} and 0.0 mM Ba^{2+}. Scale bars, 200 pA. (*B*) AMFE is observed when peak tail currents, normalized to 1.0 when $Ba^{2+}/(Ba^{2+} + Ca^{2+}) = 0$, are plotted against $Ba^{2+}/(Ba^{2+} + Ca^{2+})$. Wild-type (○), F1144G (□), FY/GK (△), and Y1152K (●). (*C*) AMFE for F1144K (●) is more pronounced than it is for wild-type (○). In *B* and *C*, identical results were obtained regardless of the order the divalent mixtures were added. Wild-type, $n = 4$; F1144G, $n = 7$; Y1152K, $n = 5$; FY/GK, $n = 4$; and F1144K, $n = 5$.

$+ Ca^{2+}) = 0.7$ before rapidly climbing to ~1.2 as $Ba^{2+}/(Ba^{2+} + Ca^{2+})$ approaches 1.0. F1144G (*squares*) and FY/GK (*triangles*) do not exhibit an AMFE. The tail current amplitudes for F1144G and FY/GK decline almost monotonically with wild-type as $Ba^{2+}/(Ba^{2+} + Ca^{2+})$ progresses to 0.7, but fail to increase as $Ba^{2+}/(Ba^{2+} + Ca^{2+})$ approaches 1.0. In contrast to F1144G and FY/GK, Y1152K (*solid circles*) exhibits a robust AMFE, demonstrating that the AMFEs for FY/GK and perhaps F1144G are, indeed, attenuated. That the relative current amplitudes for FY/GK and Y1152K are indistinguishable when $Ba^{2+}/(Ba^{2+} + Ca^{2+}) = 1$ yet only Y1152K presents an AMFE, indicates that the I_{Ba}/I_{Ca} and the AMFE can be altered independently. This point is further exemplified in Fig. 11 *C* where the AMFE for F1144K (*closed circles*) is greater than the AMFE for wild-type (*open circles*). Notice that F1144K reaches a minimum value of 0.55 compared to 0.70 for wild-type. This enhanced AMFE is not likely to be linked to changes in the binding affinities of single Ca^{2+} and Ba^{2+} ions to the pore because the binding affinities changed very little for this mutant compared to the others (see Fig. 9). Together, these results suggest that the identity of the residue at position 1144 can accentuate or attenuate the AMFE.

DISCUSSION

Phe-1144 and Tyr-1152 substitutions reduce Ba^{2+} conductance by altering electrostatic and/or chemical interactions in pores occupied by multiple ions

Our data indicate that the reductions in Ba^{2+} conductance observed with F1144G, Y1152K, FY/GK, and F1144K do not arise from changes in the binding properties of single cations to the pore for the following reasons: First, if high affinity Ba^{2+} binding were inversely related to conductance, the mutant channels' reduction in Ba^{2+} conductance would be correlated with an increased binding affinity for individual Ba^{2+} ions and not the decreases observed in our experiments (Figs. 8 and 9). Second, the IC_{50} for half-maximal block of Li^+ currents through Y1152K channels by divalent cations is larger than it is for F1144G and F1144K (Figs. 8 and 9), yet unlike the Phe-1144 mutants, the G_{Ba}/G_{Ca} for Y1152K is decreased to the smallest extent (Figs. 4–7 and 10). Third, and perhaps most significantly, although the binding affinities of individual Ca^{2+} and Ba^{2+} ions to the selectivity filters of all four mutant channels are reduced, these reductions are not ion specific—i.e., the fold change in IC_{50} values for half-maximal block of Li^+ currents by Ba^{2+} is approximately equal to that by Ca^{2+} for all four mutant channels (Fig. 9). The small ion-specific differences that do appear in Fig. 9 cannot be responsible for reduced Ba^{2+} conductance because such differences are observed with Y1152K as well. Finally, like wild-type, the concentration for half-maximal block of Li^+ currents through all the mutant channels is ~35-fold lower for Ca^{2+} than it is for Ba^{2+}. Thus, all the mutant channels would be expected to exhibit an AMFE similar to that of wild-type. Consistent with this prediction, the AMFE is preserved for Y1152K but it is not for F1144G and FY/GK, despite the fact that the effects on Li^+ block are similar between all three mutants. Thus, contrary to theoretical models that base the differences between Ba^{2+} and Ca^{2+} conductance on the energetics of high affinity binding to the selectivity filter (25–28), our data indicate that high affinity interactions between the selectivity filter and individual Ba^{2+} or Ca^{2+} ions play only a minor, if any, role in determining the AMFE or the channel's preference for conducting one ion over the other.

Instead, we observe large, ion-specific effects when the mutant pores are occupied by multiple divalent cations (Fig. 10). It is likely that G_{Ba}/G_{Ca} for wild-type is ~2 because a combination of electrostatic and/or chemical forces, all dictated by the pore geometry, act on multiple Ba^{2+} ions in ways that are quantitatively different from the way they act on Ca^{2+}

ions. In contrast, G_{Ba}/G_{Ca} for the mutant channels approaches one because these forces act on Ba^{2+} and Ca^{2+} ions more equally. If the mutant selectivity filter is unable to discriminate between Ba^{2+} and Ca^{2+}, one would predict that the AMFE would be flat, as indeed it is for F1144G and FY/GK.

Our observations that both whole-cell and unitary Ba^{2+} currents through F1144G channels are reduced compared to wild-type channels (Figs. 4–7, 10) are consistent with the results of Sather and colleagues (33), who found that the unitary conductance is proportional to the volume of the side chain introduced at position 1144. The positively charged lysine, whose Van der Waals volume is identical to that of phenylalanine, appears to be an exception to this rule. Based on the size of its substituted lysine residue, F1144K would be expected to exhibit conductance properties similar to those of wild-type. Our findings that Ba^{2+} conductance for F1144K resembles that of F1144G and not wild-type (Figs. 4–7, 10) are inconsistent with the premise that Ba^{2+} conductance is proportional to the side-chain volume at position 1144. Since Phe-1144 and Glu-1145 are neighboring amino acids that may interact (33), Glu-1145 may be held in a more restricted orientation when its neighboring residue is a positively charged lysine residue and in a less restricted orientation when its neighboring residue is a glycine residue. Thus, even though F1144G and F1144K both reduce Ba^{2+} currents, one would predict that there are subtle differences between the conductance properties of the two mutants. Such differences can be observed by comparing their respective AMFEs. When Phe-1144 is replaced with a glycine, the AMFE is flattened, whereas a lysine substitution enhances the AMFE. Thus, the AMFE is dependent on the identity of the amino acid residue at position 1144, suggesting that glycine and lysine substitutions at position 1144 reduce Ba^{2+} conductance via different mechanisms.

Phe-1144 and Tyr-1152 substitutions discussed in the context of contemporary structure-based models for Ca^{2+} channel permeation

Over the past decade an increasingly clearer picture has emerged of how the pore selectivity filter of the voltage-gated calcium channel confers high calcium selectivity while simultaneously supporting high rates of calcium flux. The EEEE locus is the critical player in this process, since it forms the calcium binding site. Nevertheless, our findings are consistent with a growing body of data suggesting that residues surrounding the EEEE locus also play important roles in fine tuning pore selectivity. Traditionally, two-site, three-barrier models based on measurable forces and binding energies have been used to describe the fundamental properties of ion selectivity and permeation through Ca^{2+} channels. These models cannot be used for structural studies because the forces and binding energies are not defined with realistic structural constraints. Newer models have been developed that reproduce many of the biophysical characteristics of ion permeation using structures thought to resemble the Ca^{2+} channel pore (57–61). Below, we discuss our experimental findings in the context of these new ''structure-based'' models.

The structural model of Lipkind and Fozzard (60), for example, can be thought of as a structural correlate to the ''step'' model of Dang and McCleskey (28) and the experimental findings of Kuo and Hess (62). In this model, the eight carboxyl groups from the EEEE locus form three binding sites: a central, high affinity divalent cation binding site formed by four of the carboxyl groups flanked by two low affinity divalent cation binding sites, each composed of two carboxyl groups. In the context of this model, our findings suggest that substitutions at positions 1144 and 1152 alter the interactions between one of the two low affinity glutamate pairs and Ba^{2+}, but not Ca^{2+}. A more detailed kinetic analysis of the mutants could reveal which of the two low affinity sites is altered.

That the selectivity filter has a defined volume is implied in the early barrier models (25,26,63), and that this volume is defined by the eight carbonyl oxygen atoms from the EEEE locus is explicit in contemporary models (11,57,59,61). Although the crystal diameters of Ca^{2+} and Na^{+} ions are nearly identical (2.00 vs. 2.04 Å, respectively), each Ca^{2+} ion carries twice as much countercharge as a Na^{+} ion. Thus, unlike Na^{+}, Ca^{2+} is able to neutralize the highly charged selectivity filter without overcrowding the pore with counterions. Although the Ba^{2+} and Ca^{2+} ions carry the same charge, the ionic diameter of Ba^{2+} is ~36% larger than that of Ca^{2+} (2.72 vs. 2.00 Å, respectively). Thus, Ba^{2+} ions would be predicted to exhibit a higher degree of crowding than Ca^{2+} ions, resulting in a faster exit rate and larger conductance for Ba^{2+}. This ''volume exclusion/charge neutralization'' model can account for our findings if it is assumed that the substitutions at positions 1144 and 1152 altered the geometry and/or electrostatic environment of the selectivity filter such that it is more amenable to support occupancy by multiple, larger Ba^{2+} ions, whereas its ability to support occupancy by multiple Ca^{2+} ions changes little, i.e., if the selectivity filters of the mutant channels were to become less susceptible to ''overcrowding'' by Ba^{2+} ions. Such Ba^{2+}-specific changes in the electrostatic-binding forces in the pore would predict that the mutant channel would exhibit a reduction in its Ba^{2+} conductance, whereas its Ca^{2+} conductance would be relatively unaffected.

Additional residues determine the permeability properties of several classes of voltage-gated Ca^{2+} channels

Here, we report that nonglutamate residues in the pore of L-type Ca^{2+} channels play critical roles in determining important properties of ion permeation. We originally hypothesized that the identity of the residues at positions 1144 and 1152 would confer subtype-specific characteristics on ion

permeation. However, all the $Ca_V2.1$-like mutant channels tested, F1144G, Y1152K, and FY/GK, exhibited conductance properties that were more similar to Ca_V3 channels than $Ca_V2.1$ channels. Therefore, residues other than those at positions 1144 and 1152 are critical for determining the permeability properties of voltage-gated Ca^{2+} channels (33). Work by others supports this conclusion. For example, a $Ca_V3.1$ mutant where Asp-1145 is replaced by glutamate exhibits a I_{Ba}/I_{Ca} that is more reminiscent of $Ca_V1.2$ than $Ca_V3.1$ (64). Furthermore, substitutions as far as 100 residues upstream of Glu-1145 in $Ca_V2.2$ (N-type) channels reduce the channel's preference for passing Ba^{2+} currents over Ca^{2+} currents (32). Discovering how the glutamate and non-glutamate residues are arranged in the pore and how this structural arrangement produces an electrostatic and chemical environment conducive to ion permeation will undoubtedly be a challenging task. The consequences of this effort will greatly expand our understanding of the molecular details underlying ion permeation.

This work was supported by research grants from the American Heart Association (0230298N) and the National Institutes of Health (RO1 HL-074143) to B.Z.P., research grants from the Canadian Institutes of Health to D.S.R. (MT-13485) and 08HL-062465, and the Oishei Foundation to R.L.R.

REFERENCES

1. Hille, B. 2001. Ion Channels of Excitable Membranes, 3rd ed. Sinaur Associates, Sunderland, MA.
2. Roux, B., and R. MacKinnon. 1999. The cavity and pore helices in the KcsA K^+ channel: electrostatic stabilization of monovalent cations. *Science*. 285:100–102.
3. Zhou, Y., J. H. Morais-Cabral, A. Kaufman, and R. MacKinnon. 2001. Chemistry of ion coordination and hydration revealed by a K^+ channel-Fab complex at 2.0 Å resolution. *Nature*. 414:43–48.
4. Morais-Cabral, J. H., Y. Zhou, and R. MacKinnon. 2001. Energetic optimization of ion conduction rate by the K^+ selectivity filter. *Nature*. 414:37–42.
5. Doyle, D. A., J. Morais Cabral, R. A. Pfuetzner, A. Kuo, J. M. Gulbis, S. L. Cohen, B. T. Chait, and R. MacKinnon. 1998. The structure of the potassium channel: molecular basis of K^+ conduction and selectivity. *Science*. 280:69–77.
6. McCleskey, E. W., and W. Almers. 1985. The Ca channel in skeletal muscle is a large pore. *Proc. Natl. Acad. Sci. USA*. 82:7149–7153.
7. Wu, X. S., H. D. Edwards, and W. A. Sather. 2000. Side chain orientation in the selectivity filter of a voltage-gated Ca^{2+} channel. *J. Biol. Chem.* 275:31778–31785.
8. Klockner, U., G. Mikala, A. Schwartz, and G. Varadi. 1996. Molecular studies of the asymmetric pore structure of the human cardiac voltage-dependent Ca^{2+} channel. Conserved residue, Glu-1086, regulates proton-dependent ion permeation. *J. Biol. Chem.* 271:22293–22296.
9. Chen, X. H., and R. W. Tsien. 1997. Aspartate substitutions establish the concerted action of P-region glutamates in repeats I and III in forming the protonation site of L-type Ca^{2+} channels. *J. Biol. Chem.* 272: 30002–30008.
10. Chen, X. H., I. Bezprozvanny, and R. W. Tsien. 1996. Molecular basis of proton block of L-type Ca^{2+} channels. *J. Gen. Physiol.* 108:363–374.
11. Ellinor, P. T., J. Yang, W. A. Sather, J. F. Zhang, and R. W. Tsien. 1995. Ca^{2+} channel selectivity at a single locus for high-affinity Ca^{2+} interactions. *Neuron*. 15:1121–1132.
12. Kim, M. S., T. Morii, L. X. Sun, K. Imoto, and Y. Mori. 1993. Structural determinants of ion selectivity in brain calcium channel. *FEBS Lett.* 318:145–148.
13. Mikala, G., A. Bahinski, A. Yatani, S. Tang, and A. Schwartz. 1993. Differential contribution by conserved glutamate residues to an ion-selectivity site in the L-type Ca^{2+} channel pore. *FEBS Lett.* 335:265–269.
14. Sather, W. A., J. Yang, and R. W. Tsien. 1994. Structural basis of ion channel permeation and selectivity. *Curr. Opin. Neurobiol.* 4:313–323.
15. Tang, S., G. Mikala, A. Bahinski, A. Yatani, G. Varadi, and A. Schwartz. 1993. Molecular localization of ion selectivity sites within the pore of a human L-type cardiac calcium channel. *J. Biol. Chem.* 268:13026–13029.
16. Yang, J., P. T. Ellinor, W. A. Sather, J. F. Zhang, and R. W. Tsien. 1993. Molecular determinants of Ca^{2+} selectivity and ion permeation in L-type Ca^{2+} channels. *Nature*. 366:158–161.
17. Yatani, A., A. Bahinski, G. Mikala, S. Yamamoto, and A. Schwartz. 1994. Single amino acid substitutions within the ion permeation pathway alter single-channel conductance of the human L-type cardiac Ca^{2+} channel. *Circ. Res.* 75:315–323.
18. Bahinski, A., A. Yatani, G. Mikala, S. Tang, S. Yamamoto, and A. Schwartz. 1997. Charged amino acids near the pore entrance influence ion-conduction of a human L-type cardiac calcium channel. *Mol. Cell. Biochem.* 166:125–134.
19. Heinemann, S. H., H. Terlau, W. Stuhmer, K. Imoto, and S. Numa. 1992. Calcium channel characteristics conferred on the sodium channel by single mutations. *Nature*. 356:441–443.
20. Yamagishi, T., M. Janecki, E. Marban, and G. F. Tomaselli. 1997. Topology of the P segments in the sodium channel pore revealed by cysteine mutagenesis. *Biophys. J.* 73:195–204.
21. Chiamvimonvat, N., M. T. Perez-Garcia, G. F. Tomaselli, and E. Marban. 1996. Control of ion flux and selectivity by negatively charged residues in the outer mouth of rat sodium channels. *J. Physiol.* 491:51–59.
22. Chiamvimonvat, N., M. T. Perez-Garcia, R. Ranjan, E. Marban, and G. F. Tomaselli. 1996. Depth asymmetries of the pore-lining segments of the Na^+ channel revealed by cysteine mutagenesis. *Neuron*. 16:1037–1047.
23. Bourinet, E., G. W. Zamponi, A. Stea, T. W. Soong, B. A. Lewis, L. P. Jones, D. T. Yue, and T. P. Snutch. 1996. The alpha 1E calcium channel exhibits permeation properties similar to low-voltage-activated calcium channels. *J. Neurosci.* 16:4983–4993.
24. Hagiwara, S., J. Fukuda, and D. C. Eaton. 1974. Membrane currents carried by Ca, Sr, and Ba in barnacle muscle fiber during voltage clamp. *J. Gen. Physiol.* 63:565–578.
25. Almers, W., and E. W. McCleskey. 1984. Non-selective conductance in calcium channels of frog muscle: calcium selectivity in a single-file pore. *J. Physiol.* 353:585–608.
26. Hess, P., and R. W. Tsien. 1984. Mechanism of ion permeation through calcium channels. *Nature*. 309:453–456.
27. Yue, D. T., and E. Marban. 1990. Permeation in the dihydropyridine-sensitive calcium channel. Multi-ion occupancy but no anomalous mole-fraction effect between Ba^{2+} and Ca^{2+}. *J. Gen. Physiol.* 95:911–939.
28. Dang, T. X., and E. W. McCleskey. 1998. Ion channel selectivity through stepwise changes in binding affinity. *J. Gen. Physiol.* 111:185–193.
29. Kostyuk, P. G., S. L. Mironov, and Y. M. Shuba. 1983. Two ion-selecting filters in the calcium channel of the somatic membrane of mollusc neuron. *J. Membr. Biol.* 76:83–93.
30. Fukushima, Y., and S. Hagiwara. 1985. Currents carried by monovalent cations through calcium channels in mouse neoplastic B lymphocytes. *J. Physiol.* 358:255–284.
31. Parent, L., and M. Gopalakrishnan. 1995. Glutamate substitution in repeat IV alters divalent and monovalent cation permeation in the heart Ca^{2+} channel. *Biophys. J.* 69:1801–1813.
32. Feng, Z. P., J. Hamid, C. Doering, S. E. Jarvis, G. M. Bosey, E. Bourinet, T. P. Snutch, and G. W. Zamponi. 2001. Amino acid residues

outside of the pore region contribute to N-type calcium channel permeation. *J. Biol. Chem.* 276:5726–5730.

33. Williamson, A. V., and W. A. Sather. 1999. Nonglutamate pore residues in ion selection and conduction in voltage-gated Ca(2+) channels. *Biophys. J.* 77:2575–2589.
34. Peterson, B. Z., and W. A. Catterall. 1995. Calcium binding in the pore of L-type calcium channels modulates high affinity dihydropyridine binding. *J. Biol. Chem.* 270:18201–18204.
35. Peterson, B. Z., C. D. DeMaria, J. P. Adelman, and D. T. Yue. 1999. Calmodulin is the Ca^{2+} sensor for Ca^{2+}-dependent inactivation of L-type calcium channels. *Neuron.* 22:549–558.
36. Peterson, B. Z., J. S. Lee, J. G. Mulle, Y. Wang, M. de Leon, and D. T. Yue. 2000. Critical determinants of Ca(2+)-dependent inactivation within an EF-hand motif of L-type Ca(2+) channels. *Biophys. J.* 78: 1906–1920.
37. Wei, X. Y., E. Perez-Reyes, A. E. Lacerda, G. Schuster, A. M. Brown, and L. Birnbaumer. 1991. Heterologous regulation of the cardiac Ca^{2+} channel alpha 1 subunit by skeletal muscle beta and gamma subunits. Implications for the structure of cardiac L-type Ca^{2+} channels. *J. Biol. Chem.* 266:21943–21947.
38. Perez-Reyes, E., A. Castellano, H. S. Kim, P. Bertrand, E. Baggstrom, A. E. Lacerda, X. Y. Wei, and L. Birnbaumer. 1992. Cloning and expression of a cardiac/brain beta subunit of the L-type calcium channel. *J. Biol. Chem.* 267:1792–1797.
39. Tomlinson, W. J., A. Stea, E. Bourinet, P. Charnet, J. Nargeot, and T. P. Snutch. 1993. Functional properties of a neuronal class C L-type calcium channel. *Neuropharmacology.* 32:1117–1126.
40. Qin, N., R. Olcese, M. Bransby, T. Lin, and L. Birnbaumer. 1999. Ca^{2+}-induced inhibition of the cardiac Ca^{2+} channel depends on calmodulin. *Proc. Natl. Acad. Sci. USA.* 96:2435–2438.
41. Zuhlke, R. D., G. S. Pitt, K. Deisseroth, R. W. Tsien, and H. Reuter. 1999. Calmodulin supports both inactivation and facilitation of L-type calcium channels. *Nature.* 399:159–162.
42. Hamill, O. P., A. Marty, E. Neher, B. Sakmann, and F. J. Sigworth. 1981. Improved patch-clamp techniques for high-resolution current recording from cells and cell-free membrane patches. *Pflugers Arch.* 391:85–100.
43. Smith, P. A., F. M. Aschroft, and C. M. Fewtrell. 1993. Permeation and gating properties of the L-type calcium channel in mouse pancreatic beta cells. *J. Gen. Physiol.* 101:767–797.
44. Hess, P., J. B. Lansman, and R. W. Tsien. 1986. Calcium channel selectivity for divalent and monovalent cations. Voltage and concentration dependence of single channel current in ventricular heart cells. *J. Gen. Physiol.* 88:293–319.
45. Fox, A. P., M. C. Nowycky, and R. W. Tsien. 1987. Single-channel recordings of three types of calcium channels in chick sensory neurones. *J. Physiol.* 394:173–200.
46. Cloues, R. K., S. J. Tavalin, and N. V. Marrion. 1997. Beta-adrenergic stimulation selectively inhibits long-lasting L-type calcium channel facilitation in hippocampal pyramidal neurons. *J. Neurosci.* 17:6493–6503.
47. Mantegazza, M., C. Fasolato, J. Hescheler, and D. Pietrobon. 1995. Stimulation of single L-type calcium channels in rat pituitary GH3 cells by thyrotropin-releasing hormone. *EMBO J.* 14:1075–1083.
48. Kokubun, S., and H. Reuter. 1984. Dihydropyridine derivatives prolong the open state of Ca channels in cultured cardiac cells. *Proc. Natl. Acad. Sci. USA.* 81:4824–4827.
49. Lacerda, A. E., and A. M. Brown. 1989. Nonmodal gating of cardiac calcium channels as revealed by dihydropyridines. *J. Gen. Physiol.* 93:1243–1273.
50. Tavalin, S. J., D. Shepherd, R. K. Cloues, S. E. Bowden, and N. V. Marrion. 2004. Modulation of single channels underlying hippocampal L-type current enhancement by agonists depends on the permeant ion. *J. Neurophysiol.* 92:824–837.
51. Caffrey, J. M., I. R. Josephson, and A. M. Brown. 1986. Calcium channels of amphibian stomach and mammalian aorta smooth muscle cells. *Biophys. J.* 49:1237–1242.
52. Bevington, P. R. 1969. Data Reduction and Error Analysis for the Physical Sciences. McGraw-Hill, Inc., New York.
53. Hess, P., J. B. Lansman, and R. W. Tsien. 1984. Different modes of Ca channel gating behaviour favoured by dihydropyridine Ca agonists and antagonists. *Nature.* 311:538–544.
54. Campbell, D. L., R. L. Rasmusson, and H. C. Strauss. 1988. Theoretical study of the voltage and concentration dependence of the anomalous mole fraction effect in single calcium channels. New insights into the characterization of multi-ion channels. *Biophys. J.* 54: 945–954.
55. Friel, D. D., and R. W. Tsien. 1989. Voltage-gated calcium channels: direct observation of the anomalous mole fraction effect at the single-channel level. *Proc. Natl. Acad. Sci. USA.* 86:5207–5211.
56. Wakamori, M., M. Strobeck, T. Niidome, T. Teramoto, K. Imoto, and Y. Mori. 1998. Functional characterization of ion permeation pathway in the N-type Ca^{2+} channel. *J. Neurophysiol.* 79:622–634.
57. Corry, B., T. W. Allen, S. Kuyucak, and S. H. Chung. 2001. Mechanisms of permeation and selectivity in calcium channels. *Biophys. J.* 80:195–214.
58. Nonner, W., and B. Eisenberg. 1998. Ion permeation and glutamate residues linked by Poisson-Nernst-Planck theory in L-type calcium channels. *Biophys. J.* 75:1287–1305.
59. Boda, D., D. Henderson, and D. D. Busath. 2001. Monte Carlo simulations of the mechanism for channel selectivity: the competition between volume exclusion and charge neutrality. *J. Phys. Chem.* 104: 11574–11577.
60. Lipkind, G. M., and H. A. Fozzard. 2001. Modeling of the outer vestibule and selectivity filter of the L-type Ca^{2+} channel. *Biochemistry.* 40:6786–6794.
61. Nonner, W., L. Catacuzzeno, and B. Eisenberg. 2000. Binding and selectivity in L-type calcium channels: a mean spherical approximation. *Biophys. J.* 79:1976–1992.
62. Kuo, C. C., and P. Hess. 1993. Ion permeation through the L-type Ca^{2+} channel in rat phaeochromocytoma cells: two sets of ion binding sites in the pore. *J. Physiol.* 466:629–655.
63. Hille, B., and W. Schwarz. 1978. Potassium channels as multi-ion single-file pores. *J. Gen. Physiol.* 72:409–442.
64. Talavera, K., M. Staes, A. Janssens, N. Klugbauer, G. Droogmans, F. Hofmann, and B. Nilius. 2001. Aspartate residues of the Glu-Glu-Asp-Asp (EEDD) pore locus control selectivity and permeation of the T-type Ca(2+) channel alpha(1G). *J. Biol. Chem.* 276:45628–45635.
65. Kuo, C. C., and P. Hess. 1993. Characterization of the high-affinity Ca^{2+} binding sites in the L-type Ca^{2+} channel pore in rat phaeochromocytoma cells. *J. Physiol.* 466:657–682.
66. Tsien, R. W., P. Hess, E. W. McCleskey, and R. L. Rosenberg. 1987. Calcium channels: mechanisms of selectivity, permeation, and block. *Annu. Rev. Biophys. Biophys. Chem.* 16:265–290.